Tellus (1998), 50A, 616–636
Printed in UK – all rights reserved

TELLUS
ISSN 0280–6495

Nonlinear adjustment of a rotating homogeneous atmosphere to zonal momentum forcing

By RONALD P. WEGLARZ* and YUH-LANG LIN *Department of Marine, Earth, and Atmospheric Sciences, North Carolina State University, Raleigh, North Carolina 27695-8208, USA*

(Manuscript received 7 October 1997; in final form 5 May 1998)

ABSTRACT

Idealized numerical simulations using a simple shallow water model are performed to study a generalized Rossby adjustment problem which focuses on the nonlinear response of a rotating, uniform, homogeneous, barotropic zonal flow to meso-α and β scale zonal momentum forcing. The prescribed forcings propagate downstream at a speed (c) which is less than the basic state flow speed (U), and represent the local effects of momentum deposition/redistribution attributable to a variety of physical processes. For small Rossby number flow and $t \leqslant \tau = 2a/(U-c)$, the near-field response to meso-α scale forcing in the moving frame of reference is to produce localized zonal jets of finite longitudinal and latitudinal extent whose geometries are similar to the imposed forcing structure. The perturbation mass (height) field adjusts to the wind field associated with these disturbances. Although the free surface vertical motion is dominated by transient inertia-gravity waves at early times, well-defined localized vertical motions also form in the vicinity of the forcing center. For *isolated* forcing, ascending and descending vertical motion occurs south and north of the forcing center, respectively. For *dipole* forcing, a four-cell pattern of vertical motion characterized by ascent in the southwest and northeast quadrants and descent in the northwest and southeast quadrants flanks the forcing center where a pair of easterly and westerly jets form. For $t > \tau$, the exit region of the localized zonal jet produced by isolated forcing is advected downstream, carrying portions of the meridional perturbation winds and free surface displacement fields with it. The long term asymptotic response is a zonally elongated, synoptic scale jet due to the temporally continuous relative vorticity generated by the zonal momentum forcing. A divergent cross-stream ageostrophic flow in the jet entrance region produces an isolated region of ascending vertical motion which is compensated by weaker regions of descent to the east and west of the forcing center. The easterly jet produced by flow deceleration in the exit region of the dipole forcing is advected downstream during the same time period. A four-cell pattern of vertical motion accompanies this easterly jet. The response in the vicinity of the forcing center is an isolated meso-α scale westerly jet, with meridionally confluent flow in its entrance region and meridionally diffluent flow in its exit region. The ageostrophic circulation produces rising motion in the jet entrance region and sinking motion in the jet exit region. For moderately large Rossby number flow and meso-β scale dipole forcing, a mesoscale cyclone forms in response to fluid parcels being displaced southward into deeper fluid around a ridge in the height field. The moderately strong meso-β scale zonal wind maximum which is produced has associated vertical motions whose geometry is similar to those produced by larger meso-α scale dipole forcing. Stronger nonlinear advection allows the meso-β scale jet to form four times sooner than the westerly jet produced by smaller Rossby number meso-α scale dipole forcing.

* Corresponding author: Department of Marine, Earth, and Atmospheric Sciences, Campus Box 8208, North Carolina State University, Raleigh, North Carolina 27695-8208, USA
e-mail: ronald_weglarz@nscu.edu

1. Introduction

Highly localized sources of momentum deposition leading to local accelerations and increased wind speeds in the atmosphere can be attributed to a variety of physical processes. Some of the more obvious and well accepted mechanisms which cause the atmosphere to either redistribute or gain additional momentum over a finite period of time are (i) the zonal force proportional to the Eliassen-Palm flux divergence induced by transient, nonlinear, Rossby wave eddy processes (Andrews and McIntyre, 1976; Pedlosky, 1987), (ii) local nonlinear eddy fluxes arising from Reynolds' stresses caused by gravity and/or inertia-gravity wave breaking producing a localized region of intense gravity wave drag (Zhu and Holton, 1987), (iii) nonlinear effects of asymmetries associated with evolving synoptic-scale waves (Challa and Pfeffer, 1980), (iv) eddy momentum fluxes associated with upper-level potential vorticity anomalies (Montgomery and Farrell, 1993), (v) the injection of a fast stream of air into the tropospheric polar or subtropical jet stream accompanying the "ventilation" or outflow of deep, organized, meso-α/β scale convection (Shutts, 1994, Shutts and Gray, 1994), and (vi) large-scale nonlinear inertial-advective accelerations accompanying the downstream propagation of midlatitude jet streaks (jets of finite latitudinal and longitudinal extent) embedded in synoptic-scale baroclinic waves that move along the polar and subtropical jet streams (Weglarz and Lin, 1997).

How the atmosphere responds in terms of its transient evolution and the subsequent approach to a newly balanced asymptotic equilibrium state to such momentum redistribution and deposition processes has been a problem of particular significance to geophysical fluid dynamicists ever since the pioneering work on geostrophic adjustment by Rossby (1938) and Cahn (1945). Blumen (1972) provides a detailed review of the early literature, while Weglarz (1994) also reviews more contemporary studies.

Although previous studies employing either analytical or numerical models of varying complexity have addressed in some detail the atmospheric response to the aforementioned momentum deposition mechanisms, little has been done in order to specifically focus on the development of the dynamically important ageostrophic circulations and vertical motions accompanying localized jets that have either been predicted theoretically or simulated numerically in previous *barotropic* geostrophic adjustment studies.

In order to bridge this gap, in this paper we study a generalized nonlinear Rossby adjustment problem within the context of shallow water dynamics wherein the response of a uniform, geostrophically balanced, barotropic zonal flow to propagating isolated and dipole meso-α and β scale momentum sources is investigated through idealized numerical model experiments using a simple shallow water model. The *prescribed* momentum forcings are taken to represent, in a highly idealized and very simple way, some of the aforementioned physical processes responsible for localized momentum deposition in the atmosphere.

Although barotropic models contain relatively simple physics, for problems not constrained by channel model geometry (Staniforth et al., 1993) or wave trapping criteria for normal mode solutions (Zhang and Webster, 1989), inclusion of a geostrophically balanced basic state flow causes the associated mathematical problem (Weglarz, 1994) to become difficult to solve analytically. This is because the coefficients of wave equations of the form given by eq. (3.6.9) of Pedlosky (1987), which govern the small-amplitude perturbations, are no longer constant. Due to the mathematical complexity imposed by a dynamically consistent set of governing equations in the presence of a nonresting basic state, we formulate and use a barotropic shallow water model employing simple numerical methods to solve the geostrophic adjustment problem associated with a moving zonal momentum source in a rotating homogeneous atmosphere.

This work is a natural extension of, and complementary to, the corresponding linear shallow water geostrophic adjustment theory for prescribed zonal momentum sources developed by Weglarz (1994) which has recently been extended theoretically by Weglarz and Lin (1997) to a continuously stratified barotropic zonal flow.

Despite the fact that geophysical fluid flows can be highly baroclinic, the overwhelming success of barotropic shallow water models to elucidate the fundamental physics of a majority of large-scale motions (Blumen, 1972; Gill, 1982) encourages us,

in a first approach, to adopt this simplest geophysical fluid dynamics model in order to isolate and clearly distinguish the ageostrophic circulations and accompanying vertical motions associated with the local momentum redistribution and deposition processes, (i)–(vi), from those associated with other features (e.g. upper-tropospheric fronts) that are often simulated in more complicated baroclinic models initialized with observed data.

The nonlinear shallow water model used in this study is presented in Section 2. Section 3 discusses the results produced by isolated zonal momentum forcing, and Section 4 discusses the results produced by dipole zonal momentum forcing. Dipole forcing more appropriately represents entrance region acceleration and exit region deceleration which the basic state zonal flow experiences as it passes through the forcing region, and therefore should be a useful first approach to understanding, for example, the zonal momentum redistribution which occurs in the real atmosphere as an isolated midlatitude jet streak propagates downstream in the background synoptic scale flow. Section 5 summarizes the major results and offers directions for future research.

2. The barotropic shallow water model

The North Carolina State University Shallow Water Model (NCSU SWM) governs finite-amplitude hydrostatic perturbations in a rotating, homogeneous atmosphere of finite depth $H(y)$ on an f-plane forced by mass, momentum, or orography. We are interested in the response of a uniform zonal flow to a localized momentum forcing traveling downstream at the the speed $c < U$ in the zonal direction. Therefore, we invoke a standard Galilean transformation such that in the transformed reference frame the propagating momentum forcing is stationary. Further, we assume that the basic flow is inviscid, mass is conserved, and the bottom topography is flat. Under these constraints, the evolution of finite-amplitude perturbations in the uniformly translating reference frame of the zonal momentum forcing will be governed by:

$$\frac{\partial u'}{\partial t} + (U-c)\frac{\partial u'}{\partial x} + u'\frac{\partial u'}{\partial x} + v'\frac{\partial u'}{\partial y} - fv' + g\frac{\partial h'}{\partial x} = F_u(\boldsymbol{r}), \tag{1}$$

$$\frac{\partial v'}{\partial t} + (U-c)\frac{\partial v'}{\partial x} + u'\frac{\partial v'}{\partial x} + v'\frac{\partial v'}{\partial y} + fu' + g\frac{\partial h'}{\partial y} = 0, \tag{2}$$

$$\frac{\partial h'}{\partial t} + (U-c)\frac{\partial h'}{\partial x} + v'\frac{\mathrm{d}H}{\mathrm{d}y} + u'\frac{\partial h'}{\partial x} + v'\frac{\partial h'}{\partial y} + [H(y)+h']\left[\frac{\partial u'}{\partial x} + \frac{\partial v'}{\partial y}\right] = 0, \tag{3}$$

where $\boldsymbol{r} = (x, y)$ and $F_u(\boldsymbol{r})$ is the zonal momentum forcing. An f-plane approximation is adopted and the uniform basic state zonal flow is assumed to be time-independent and geostrophically balanced. Although the model is fully nonlinear, the mass and momentum fields are partitioned into basic and perturbation states so that nonlinear effects can easily be investigated.

Eqs. (1)–(3) are discretized and numerically integrated over an unstaggered grid in the Cartesian coordinates $(\boldsymbol{r}, t)$. The horizontal derivatives are approximated by fourth-order centered finite differences, and the Eulerian time tendencies are approximated by leapfrog differencing for every time step except the first, which is computed by forward differencing. Zero gradient conditions, $\phi_b^\tau = \phi_{b-1}^{\tau-1}$ (Pielke, 1984), where b represents the lateral boundary, and ϕ is any one of the model's three prognostic variables (u', v', and h'), are imposed at the lateral boundaries. Both spatial (Shapiro, 1970) and temporal (Asselin, 1972) filtering are performed at every time step throughout the numerical integration in order to remove both short and high frequency wave modes. Further details of the numerical schemes employed can be found in Weglarz (1994).

Notice that the meridional gradient in the basic height field which balances the uniform zonal flow is $\mathrm{d}H(y)/\mathrm{d}y = -f(U+c)/g$ in this reference frame. In a two-layer shallow water system, the density difference between the two layers can be incorporated by introducing a reduced gravity, $g' = g[(\rho_0 - \rho_1)/\rho_1]$, where g is the acceleration due to gravity and ρ_1 and ρ_0 denote the densities of the upper and lower layers, respectively. For a uniform zonal current, a smaller reduced gravity implies

that the meridional gradient of the basic height field (i.e., the meridional pressure gradient) must be larger to maintain the basic state geostrophic balance. Therefore, we can expect the contribution from the $v'\,\mathrm{d}H(y)/\mathrm{d}y$ term in the continuity equation to the vertical motion to be larger in a two-layer system with significantly different densities rather than in the single layer system we are considering here. This term, which physically represents the advection of the basic state height field by the meridional wind perturbation, is one of the terms sometimes referred to collectively as the "non-Doppler effect" in equatorial dynamics studies (Zhang and Webster, 1989, 1992; Zhang, 1993).

3. Response of a uniform geostrophic zonal flow to propagating isolated zonal momentum forcing

In this section, we present results showing the finite-amplitude perturbations excited by a traveling zonal momentum forcing of the form:

$$F_u(\boldsymbol{r}, t) = \frac{u_{j0}}{\tau}\left[\frac{(x-ct)^2}{a^2} + \frac{y^2}{b^2} + 1\right]^{-3/2}. \qquad (4)$$

This forcing is constrained to propagate downstream at the speed $c < U$, but is stationary in a frame of reference traveling at the speed c. All results are described with respect to this frame of reference. In this case, u_{j0} is taken to be 30 ms^{-1}, the zonal and meridional half-widths, a and b, respectively, are each equal to 500 km (therefore the forcing is meso-α scale), and the time scale τ which represents the time it takes a fluid parcel to pass through the region of greatest zonal acceleration is taken to be $2a/(U-c)$. The magnitude of the basic state zonal flow is $U = 20\ \mathrm{ms}^{-1}$, while the propagation speed of the momentum forcing is taken to be $c = 10\ \mathrm{ms}^{-1}$. The basic state height field which balances the uniform zonal current is given by $H(y) = H_0 - [f(U+c)/g]y$, where H_0, the mean unperturbed layer depth, is taken to be 8 km and can be thought of as the scale height for a homogeneous atmosphere whose surface temperature is approximately 273 K. The computational domain contains 256×256 grid points, with a grid interval of 100 km in both spatial coordinates. The time step is taken to be 60 s, and the Coriolis parameter f has the constant value $10^{-4}\ \mathrm{s}^{-1}$. It should also be noted that $|u_{j0}| > |U|$ and $|c| < |U|$.

3.1. Unbalanced transient dynamics

Fig. 1 shows the nonlinear response at $t = 4$ h in the moving frame. An isolated region of perturbation zonal flow exists in the vicinity of the forcing center, with regions of cyclonic flow north of the main jet core and anticyclonic flow south of the jet center (Fig. 1a). This localized zonal flow anomaly has a length of approximately 960 km, a width of 800 km, and a geometry similar to that of the zonal momentum forcing (Eq. (4)), which is due to the initial response ($\partial u'/\partial t_F$) to F_u. The subscript "F" on $\partial u'/\partial t$ signifies that this acceleration comes from the prescribed forcing F_u. The center of this localized zonal jet is colocated approximately with the center of the forcing. Confluent flow exists within the forcing entrance region, while diffluent flow exists in the exit region. Fig. 1a also shows the vertical motion, which is defined as

$$\begin{aligned} w' = \mathrm{D}h'/\mathrm{D}t &= \partial h'/\partial t + (U-c)\partial h'/\partial x \\ &\quad + u'/\partial h'/\partial x + v'\,\mathrm{d}H(y)/\mathrm{d}y + v'\,\partial h'/\partial y \\ &= -[H(y)+h'](\partial u'/\partial x + \partial v'/\partial y), \end{aligned}$$

at $t = 4$ h. At this time, clearly evident are radially propagating free surface inertia-gravity waves (IGWs) with centers of ascent and descent located roughly 3840 km east and west of the forcing center. Therefore, their phase speed is approximately $c_p \sim 3840\ \mathrm{km}/4\ \mathrm{h} = 266.67\ \mathrm{ms}^{-1}$. Although these transient IGWs are the dominant feature in the vertical motion field at the free surface at this time, an isolated region of subsidence north of the zonal jet core is becoming established, while a localized region of ascent is developing south of the jet core (Fig. 1a). This *implies* that the ageostrophic perturbation winds in the forcing region at this time are dominated by a northerly flow component and is the physical mechanism responsible for transferring mass from the cyclonic to the anticyclonic side of the zonal wind perturbation.

Since transient inertia-gravity wave activity still constitutes a major portion of the flow response at this time, portions of the horizontal gradients in the free surface displacement are responsible

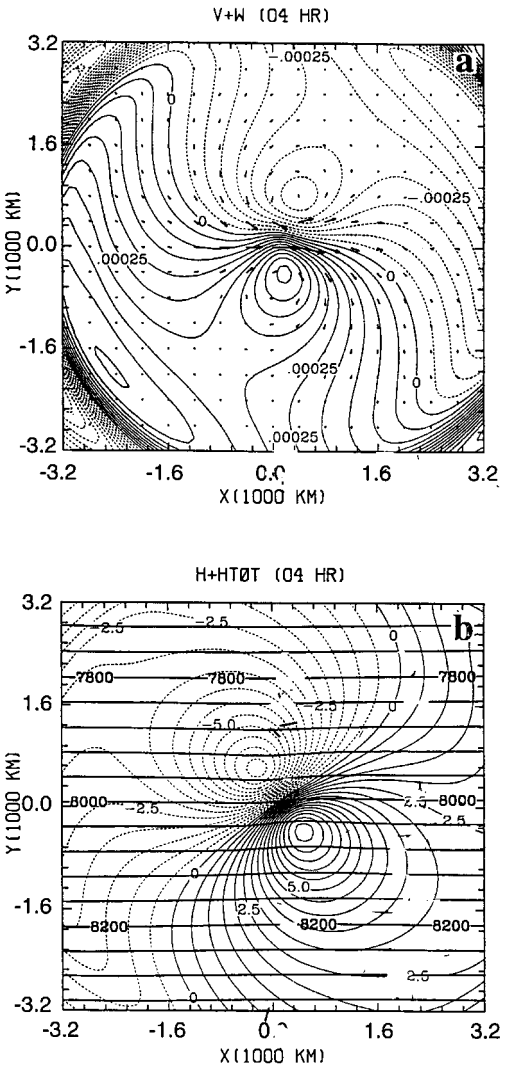

Fig. 1. (a) Total perturbation vector winds $\mathbf{V}'$ superimposed on vertical velocity w', and (b) free surface displacement h' superimposed on total free surface displacement $h = H(y) + h'$ characterizing the meso-α scale ($a = b = 500$ km, $u_{j0} = 30\ \mathrm{ms}^{-1}$) response at $t = 4$ h as seen by a Galilean observer traveling at the speed $c < U$ due to the isolated zonal momentum forcing of eq. (4). The maximum vector wind is $1.74\ \mathrm{ms}^{-1}$. The contour interval for $w'(h')$ is $9.0 \times 10^{-5}\ \mathrm{ms}^{-1}$ (0.9 m).

for supporting the winds in the IGW flow, and therefore a partitioning of the total zonal and meridional wind perturbations into geostrophic and ageostrophic components at this time is not rigorously valid. This is especially true since the free surface displacement in our model is not partitioned as $h' = h'_{\mathrm{g}} + h'_{\mathrm{ag}}$. Once the transient IGWs propagate out of the domain, a partitioning of the zonal and meridional wind perturbations will be done in order to separate the geostrophic and ageostrophic circulations induced by the prescribed zonal momentum forcing.

Fig. 1b shows that localized regions of positive and negative free surface displacement have, at $t = 4$ h, a predominantly northwest to southeast orientation due to rotational effects, and are becoming established to support the perturbation flow as the mass field (h') adjusts to the wind field (u', v'). Initially, the localized region of low free surface elevation shown in Fig. 1b is located to the west of the forcing center, and is due to divergence in the entrance region of the positive zonal wind anomaly which is produced by alongstream acceleration due to zonal momentum forcing, $\partial u'/\partial t_F = F_u$. Similarly, the localized region of high free surface elevation located to the east of the forcing center is due to convergence in the exit region of the wind anomaly. Fig. 1b represents an intermediate stage in the adjustment of the mass field dipole to establish a geostrophic balance to support the forced zonal wind anomaly (Fig. 2b). These perturbation height rises and falls have magnitudes of ~ 7.2 m at this time ($t = 4$ h), and therefore are almost undiscernable with respect to the basic state height field (Fig. 1b). Since the horizontal scale of the momentum forcing is much less than the minimum Rossby radius of deformation ($L_{\mathrm{R,min}} = [gH_{\mathrm{min}}(y)]^{1/2}/f \sim 2800$ km), the numerically simulated nonlinear response indicates that the mass field adjusts to the momentum field, in agreement with the results of linear *unforced* adjustment theory (Rossby, 1938; Cahn, 1945; Blumen, 1972; Weglarz, 1994).

3.2. *Total, geostrophic, and ageostrophic meso-α scale flow evolution*

Fig. 2a shows the total perturbation vector wind $\mathbf{V}' = u'\mathbf{i} + v'\mathbf{j}$ superimposed on w' at $t = 24$ h. At this time, the maximum wind speed associated with the forced zonal jet has increased to $\sim 8.67\ \mathrm{ms}^{-1}$. The center of this localized zonal jet is displaced downstream with respect to the stationary forcing center located at $\boldsymbol{r} = (0, 0)$ by a

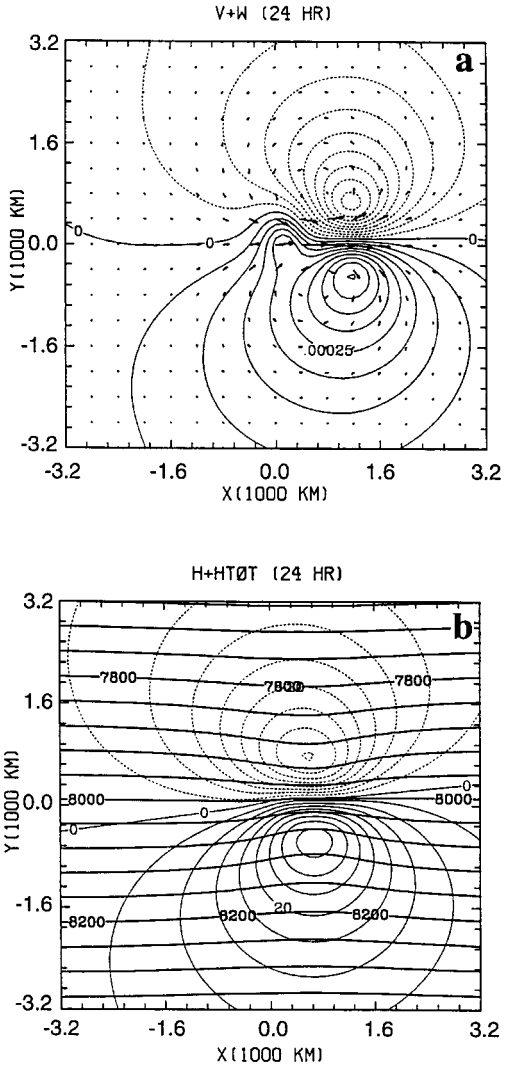

Fig. 2. Same as Fig. 1 except at $t = 24$ h. The maximum vector wind is 8.67 ms^{-1}. The contour interval for w' (h') is 5.0×10^{-5} ms^{-1} (4.0 m).

distance of $\sim$960 km. The length and width of the isolated zonal jet at this time are approximately 2080 km and 800 km, respectively. We can estimate the along-stream, L_x, and cross-stream, L_y, length scales of the jet at $t = 24$ h by the following simple analytic expressions:

$$u'_F \sim \int_0^t \frac{\partial u'_F}{\partial t}\,\mathrm{d}t \sim \int_0^t F_u\,\mathrm{d}t \sim \frac{L_x}{\Delta t}, \tag{5}$$

such that

$$L_x \sim \left(\int_0^t F_u\,\mathrm{d}t\right)(\Delta t) \sim \left\{\frac{u_{j0}}{\left[\dfrac{2a}{(U-c)}\right]}\right\}(\Delta t)^2$$

$$\sim 2240 \text{ km}, \tag{6}$$

where $u_{j0} = 30$ ms^{-1}, $a = 500$ km, $U = 20$ ms^{-1}, $c = 10$ ms^{-1}, and $\Delta t = 24$ h. Similarly, for the meridional length scale, we may estimate

$$L_y \sim \left(\int_0^t \left|-\frac{\partial h'}{\partial y}\right|\mathrm{d}t\right)(\Delta t) \sim \left(\frac{\Delta h'}{\Delta y}\right)(\Delta t)^2$$

$$\sim 560 \text{ km}, \tag{7}$$

where $|-\partial h'/\partial y| \sim 24$ m/320 km at $t = 24$ h. These simple analytical estimates are in good agreement with the numerically simulated values obtained from an analysis of Fig. 2. Note that the time-integrated prescribed momentum forcing F_u dominates the jet zonal length scale, L_x, while the evolving meridional height gradient $|-\partial h'/\partial y|$ due to geostrophic adjustment dominates the jet meridional length scale, L_y.

Fig. 2a also shows the vertical velocity field at $t = 24$ h. A well-defined, asymmetric dipole of subsidence and ascent of $\sim 4.6 \times 10^{-4}$ ms^{-1} exists in the exit region of the zonal jet. Upstream of the jet core, an isolated region of weak ascent is developing in the vicinity of the forcing center across $y = 0$. The strengthening zonal jet is flanked by two well-defined cyclonic and anticyclonic circulations north and south of $y = 0$ (Fig. 2a). These circulations are associated with the dipole of free surface displacement (Fig. 2b) which is becoming established to balance the localized zonal jet. The maximum amplitude in each cell of the dipole is $\sim$33 m, and the entire pattern is oriented in a more north-south direction across the zonal jet core at this time. The tightening meridional height gradient is a natural consequence of the mass field increasing to support the strengthening zonal jet due to continued acceleration by the prescribed momentum forcing. The meridional wind perturbation v' at this time (not shown) exhibits a four-cell pattern which characterizes confluent flow in the jet entrance region and diffluent flow in the jet exit region.

Figs. 3a and b show the geostrophic $\mathbf{V}'_g$ and

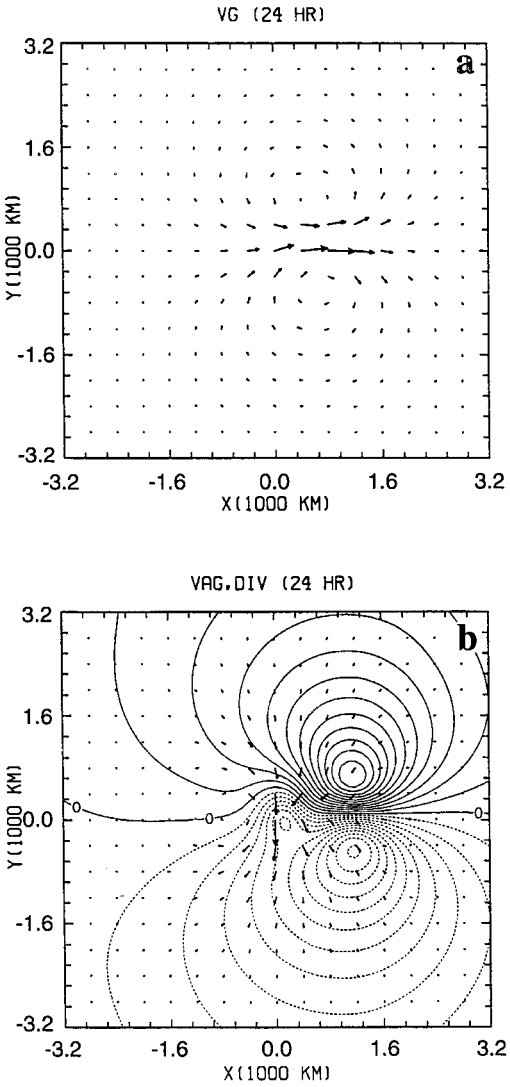

Fig. 3. (a) $\mathbf{V}'_g$, and (b) $\mathbf{V}'_{ag}$ superimposed on perturbation divergence $\delta' = (\partial u'/\partial x + \partial v'/\partial y)$ at $t = 24$ h associated with the response produced by the zonal momentum forcing of eq. (4). The maximum geostrophic (ageostrophic) vector wind is 8.48 (1.17) ms^{-1}. The contour interval for δ' is $7 \times 10^{-9}\ \mathrm{s}^{-1}$.

ageostrophic $\mathbf{V}'_{ag}$ perturbation vector winds at $t =$ 24 h, respectively, whose components are defined as $(u'_g, v'_g) = [-g/f)\,\partial h'/\partial y,\ (g/f)\,\partial h'/\partial x]$, and $(u'_{ag}, v'_{ag}) = (u' - u'_g, v' - v'_g)$, respectively. The perturbation divergence field, $\delta' = (\partial u'/\partial x + \partial v'/\partial y)$ is superimposed on $\mathbf{V}'_{ag}$ in Fig. 3b. Since the transient IGWs have propagated well outside the forcing region by this time, this type of partitioning allows the evolution of both the primary (geostrophic) and secondary (ageostrophic) circulations associated with the jet to be identified. Fig. 3a shows that the isolated jet of Fig. 2a is essentially a geostrophic zonal jet. The core of this geostrophic jet coincides with that of the total zonal jet. It is also evident from the geostrophic vector winds (Fig. 3a) that the cyclonic and anticyclonic circulations which flank the isolated zonal jet at this time (Fig. 2a) are signatures of the strengthening dipole in the free surface displacement field (Fig. 2b).

A northerly meridional ageostrophic flow forms at the entrance region of the zonal jet (Fig. 3b). The maximum wind associated with this cross-stream flow is $\sim 1.2\ \mathrm{ms}^{-1}$. This northerly ageostrophic flow is flanked by cyclonic flow to the east and anticyclonic flow to the west (Fig. 3b), which produces convergence across $y = 0$, and is therefore the physical mechanism responsible for the isolated region of vertical motion developing in the vicinity of the forcing center (Fig. 2a). Since $w' = -(\partial u'_{ag}/\partial x + \partial v'_{ag}/\partial y)z$, and the perturbation winds are independent of height, $w' > 0$ (< 0) in regions of convergence (divergence) at any level above the flat bottom throughout the entire depth of the shallow homogeneous fluid. The magnitude of this vertical motion is a linear function of height, with the maximum amplitude occuring at the free surface (Pedlosky, 1987).

The forced divergent ageostrophic flow responsible for producing the vertical motion, has a simple explanation: eastward momentum forcing leads to a southwards ageostrophic flow which produces a westward Coriolis force which tends to balance the imposed zonal momentum forcing. Compensating ageostrophic circulations are then generated outside the forcing region which satisfy the continuity equation, (3). Isolated regions of divergence north and convergence south of $y = 0$ (Fig. 3b) form approximately 1120 km downstream of $\boldsymbol{r} = (0, 0)$, and are responsible, respectively, for the subsidence and ascent in the jet exit region (Fig. 2a).

3.3. *Meso-α scale vertical motion development*

At $t = 48$ h (Fig. 4), the magnitude of the jet core has strengthened to 12.4 ms^{-1}, and has prop-

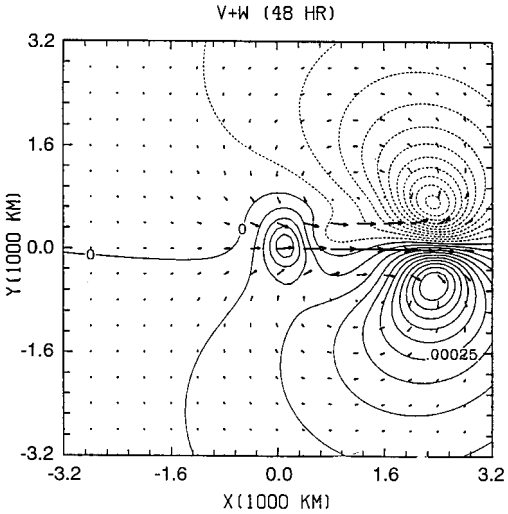

Fig. 4. $\mathbf{V}'$ superimposed on w' associated with the response for the isolated momentum forcing of eq. (4) at $t = 48$ h. The maximum total perturbation vector wind is 12.4 ms^{-1}. The contour interval for w' is 6.0×10^{-5} ms^{-1}.

agated 1280 km downstream of the forcing center. By this time, the length of this isolated jet has increased to 2560 km. The vertical motion still exhibits a dipole structure of ascent and descent in the jet exit region, although an isolated region of relatively weak ascent is now clearly colocated with the forcing center at $\boldsymbol{r} = (0, 0)$ (compare Figs. 2a, 4). The magnitude of the exit region pair are 5.5×10^{-4} ms^{-1}, while the single cell of rising motion in the jet entrance region has a magnitude of roughly 1.8×10^{-4} ms^{-1}. This vertical motion field is produced by convergence and divergence of the forced ageostrophic flow as explained in Subsection 3.2. The magnitude of the total zonal wind perturbation u' at $t = 48$ h (not shown) has increased to 13 ms^{-1}, whose compensating easterly zonal counter currents flanking the isotach maximum have magnitudes of roughly 1.9 ms^{-1}. The total height field (not shown) shows further tightening of the meridional gradient across the isolated zonal jet core, which indicates strengthening of the high-low dipole in free surface displacement which supports the strengthening geostrophic zonal wind perturbation.

The horizontal structure of the geostrophic and ageostrophic components of the perturbation flow at this time is very similar to the corresponding fields shown at $t = 24$ h (Fig. 3), except that the magnitudes of the geostrophic zonal and ageostrophic meridional flow are, respectively, 12.3 and 1.15 ms^{-1} at this time. The length and width of the geostrophic zonal jet is the same as that characterizing the total zonal flow perturbation.

$\mathbf{V}'_{ag}$ (not shown) indicates that in addition to a cross-stream ageostrophic flow colocated with the forcing center, a weaker northerly ageostrophic cross-stream flow exists downstream in the jet exit region at $x = 2240$ km. This location coincides with the dipole in vertical motion (Fig. 4). This portion of the total ageostrophic response is also present at $t = 24$ h, and is colocated with the position of the dipole in vertical motion at $x = 1120$ km (Figs. 2a, 3b).

3.4. Synoptic scale flow response at day 4

Fig. 5 shows $\mathbf{V}'$ and w' at $t = 96$ h. By this time, the core strength of the jet has increased to 13.9 ms^{-1}, and since its length has further increased to 5140 km, it may be classified as an elongated zonal wind maximum. This is inferred from the horizontal structure of the zonal wind perturbation u' (not shown). At this stage, the β-effect may start to influence the flow response, and should be considered. Although this is beyond the scope of the present paper, the effect of variable

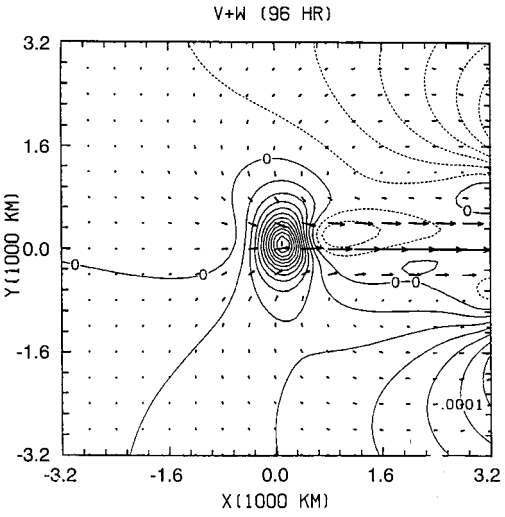

Fig. 5. Same as Fig. 1a except at $t = 96$ h (4 days). The maximum vector wind is 13.9 ms^{-1}. The contour interval for w' is 8.0×10^{-5} ms^{-1}.

Coriolis parameter (β-effect) on this forced geostrophic adjustment problem will be addressed in a forthcoming companion paper.

The first 3200 km of the $\mathbf{V}'$ field is shown in Fig. 5, and encompasses the portion of the jet between its entrance and maximum wind regions. The width of this zonal jet is approximately 850 km. The meridional gradient in the total free surface displacement across the forced zonal jet maximum (inferred from u' to be located at $x =$ 3200 km) is about 20 m/100 km. Compensating easterly perturbation zonal winds flanking the westerly zonal jet core have centers located at $x =$ 3840 km and also continue to propagate downstream along with the jet exit region. The isolated dipole in vertical motion located in the jet exit region at $t = 48$ h still accompanies the downstream-extending jet, and is, by this time ($t =$ 96 h), approximately 4800 km east of the forcing center. The magnitude of this vertical motion dipole is $7.0 \times 10^{-4}\,\mathrm{ms}^{-1}$. The magnitude of the isolated cell of rising motion colocated with the forcing center in the jet entrance region is roughly $2.43 \times 10^{-4}\,\mathrm{ms}^{-1}$, and is flanked by an isolated region of compensating subsidence centered at $\boldsymbol{r} =$ (1120 km, 160 km). The increasing downstream growth of the forced zonal jet is simply a consequence of the downstream advection of the temporally continuous relative vorticity generated by the zonal momentum forcing by the uniform basic flow.

Analysis of the individual terms in the continuity equation (not shown) indicates that the advection of the free surface displacement by the reduced zonal flow, $-(U-c)\,\partial h'/\partial x$, and the advection of the basic state height field by the meridional wind perturbation, $-v'\,\mathrm{d}H(y)/\mathrm{d}y$, have identical horizontal structures, and therefore tend to cancel each other's contribution to the field of vertical motion. The horizontal structure in $-(U-c)\,\partial h'/\partial x$ is a natural consequence of the high-low dipole in the free surface displacement field that geostrophically balances the zonal and meridional perturbation wind fields. Furthermore, the horizontal structure in $-v'\,\mathrm{d}H(y)/\mathrm{d}y$ is a natural consequence of the four-cell pattern of perturbation meridional wind v' (not shown) which defines confluence in the entrance and diffluence in the exit region of the forced zonal jet.

For the particular parameters chosen here which characterize the basic state as well as the magnitude and propagation speed of the prescribed momentum forcing, the nonlinear advection of the free surface displacement by the zonal and meridional wind perturbations, $-(u'\,\partial h'/\partial x + v'\,\partial h'/\partial y)$, have geometries and magnitudes which tend to cancel their contributions to the vertical motion. Contribution from the linear divergence term, $-H(y)(\partial u'/\partial x + \partial v'/\partial y)$, dominates the contribution from the corresponding nonlinear term, $-h'(\partial u'/\partial x + \partial v'/\partial y)$, and is associated with the isolated cross-stream ageostrophic meridional flow at $\boldsymbol{r} = (0, 0)$.

The vertical motion at the free surface (Fig. 5) obtains its horizontal structure essentially from two primary, contributing factors, each one being important at different times during the evolution to forced equilibrium. For $t \leqslant 24$ h, the first is the local tendency in the free surface displacement, $\partial h'/\partial t$. This mechanism produces a high-low dipole across $y = 0$ and is associated with the lowering of the free surface on the cyclonic side and raising of the free surface on the anticyclonic side of the isolated zonal jet as the perturbation mass field adjusts to the perturbation wind field in order to establish a geostrophically balanced equilibrium. Since the dipole in h' propagates downstream in order to maintain the geostrophic balance of the lengthening zonal jet, then the $\partial h'/\partial t$ contribution to the vertical motion within the vicinity of the forcing center at $\boldsymbol{r} = (0, 0)$ diminishes over time. The second is the non-zero contribution from the sum of the individual terms which physically represent either linear or nonlinear advective or divergence processes in eq. (3), and is important for $t > 24$ h. The non-zero sum of these terms is responsible for the divergent meridional cross-stream northerly ageostrophic perturbation flow which exists in the jet entrance region and is colocated with the forcing center. The strong convergence produced by this ageostrophic flow at $y = 0$ is responsible for the isolated region of positive vertical motion at the origin.

For the parameters adopted here, nonlinear contributions to the divergent ageostrophic flow are relatively insignificant. The geostrophic and ageostrophic components of the flow at this time (not shown) confirm that the forced zonal jet is primarily a geostrophic jet whose center is colocated with the center of the total zonal wind perturbation (Fig. 5).

We have shown that prescribed, isolated, meso-

α scale zonal momentum forcing, eq. (4), produces a zonally-oriented meso-α scale jet at early times ($t < 24$ h) since $\partial u'/\partial t_F \sim F_u$. Since the length scale of the forced zonal wind perturbation is less than the minimum Rossby radius of deformation $L_{R,\min} = [gH_{\min}(y)]^{1/2} \sim 2800$ km during this time period, the perturbation mass (height) field adjusts to the perturbation wind field. The imposed momentum forcing induces ageostrophic flow perturbations, from which the Coriolis force tends to compensate for and balance the imposed forcing. Compensating ageostrophic flow perturbations are then generated outside the forcing region due to the constaint imposed by mass continuity. However, the long-term ($24 \text{ h} < t \leqslant 96$ h) asymptotic behavior predicted by our numerical model tends to produce a downstream-extending jet *stream* rather than an isolated jet *streak* due to the temporally continuous relative vorticity imparted to the basic state flow by the prescribed forcing. In an attempt to produce such a response, we investigate a different type of forcing which more accurately reflects entrance (exit) region acceleration (deceleration) experienced by the basic state flow as it propagates through a developing isotach maximum. This problem is formulated in the next section.

4. Response of a uniform geostrophic zonal flow to a propagating dipole of zonal momentum forcing

In this section, we consider the response to a zonal momentum forcing of the form:

$$F_u(\boldsymbol{r}, t) = U^* \frac{\partial}{\partial x}\left[u_{j0} \left\{ \frac{(x-ct)^2}{a^2} + \frac{y^2}{b^2} + 1 \right\}^{-3/2} \right], \tag{8}$$

which is simply the alongstream gradient of the prescribed zonal momentum forcing given by eq. (4). As in Section 3, all results will be interpreted as those seen from a moving frame traveling at the speed $c < U$. The magnitude of the applied forcing, u_{j0}, as well as the zonal and meridional half-widths, a and b, respectively, are taken to be the same as those used in Section 3. U^* is a characteristic value of the basic state geostrophic zonal current through which the momentum forcing is propagating, and therefore has the value of $U - c$ for a Galilean observer. Eq. (8) may physically represent, for example, the entrance (exit) region acceleration (deceleration) of the basic state flow U^* passing through a developing zonal isotach maximum (jet streak) traveling at a speed c. Note that $|U^*| < |c|$.

4.1. Unbalanced transient dynamics

Fig. 6 shows the numerically simulated response at $t = 4$ h in the moving frame. The perturbation winds $\mathbf{V}'$ at this time (Fig. 6a), show the existence of an isolated westerly zonal jet west of the forcing center at $\boldsymbol{r} = (0, 0)$ and an isolated easterly zonal jet east of the forcing center. These jets are the initial response $\partial u'/\partial t_F = F_u$ to the imposed forcing, eq. (8). Also evident are isolated southerly and northerly jets, respectively, north and south of $y = 0$ which in part are due to the convergence generated between the localized westerly and easterly zonal jets. The isolated westerly zonal jet is flanked by cyclonic and anticyclonic circulations north and south of the forcing center (Fig. 6a), while the easterly jet is flanked by anticyclonic and cyclonic circulations north and south of the forcing center. This pairing of isolated positive and negative zonal wind perturbations west and east of the forcing center and their corresponding isolated cross-stream southerly and northerly meridional wind perturbations yield cyclonic and anticyclonic circulations in the northwest/southeast and southwest/northeast quadrants flanking the forcing center (Fig. 6a), respectively.

Fig. 6a also shows w' at the free surface at $t = 4$ h. Although transient IGWs are clearly evident, notice that a four-cell pattern is becoming established in the vicinity of the forcing center. At this time, the localized regions of ascent west of and descent east of $x = 0$ south of $y = 0$ clearly dominate the weaker cells of ascent east of and ascent west of $x = 0$ located to the north of $y = 0$, and have magnitudes of $5.3 \times 10^{-4}\,\text{ms}^{-1}$ and $5.9 \times 10^{-4}\,\text{ms}^{-1}$, respectively. Although a direct partitioning of the total zonal and meridional wind perturbations into geostrophic and ageostrophic components is not rigorously valid at this time due to the presence of significant transient IGW activity, the developing four-cell pattern of vertical motion is indirect evidence for, and results from, the development of a northerly cross-stream ageostrophic component of the total meridional

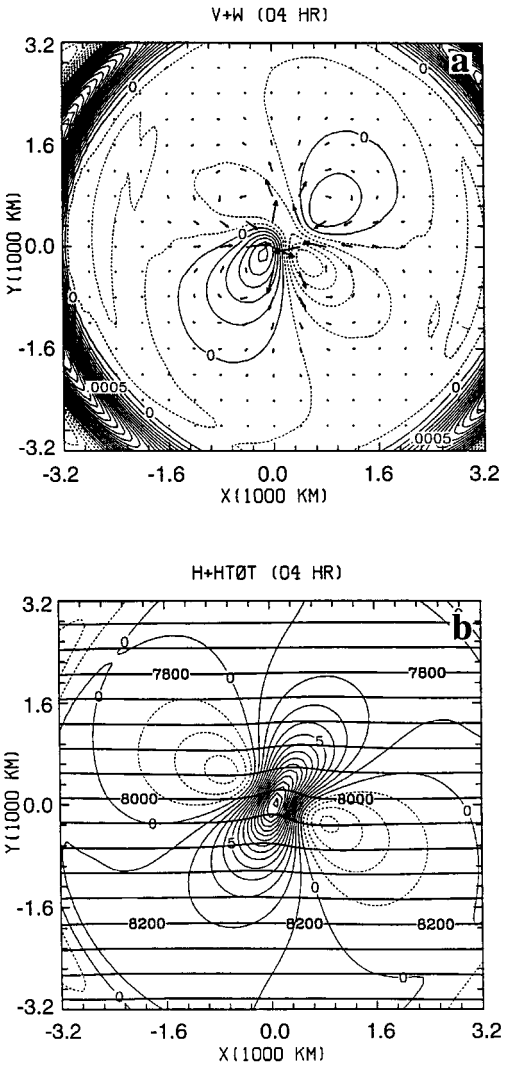

Fig. 6. Same as Fig. 1 except induced by the zonal acceleration/deceleration dipole forcing of eq. (8). The maximum vector wind is 1.74 ms^{-1}. The contour interval for w' (h') is 1.0×10^{-4} ms^{-1} (1.0 m).

wind perturbation west of and southerly cross-stream ageostrophic component east of the forcing center. The resulting divergence in the northwest and southeast quadrants and convergence in the southwest and northeast quadrants flanking $\boldsymbol{r} = (0, 0)$ due to this developing ageostrophic flow, is the primary physical mechanism responsible for the developing vertical motion field shown in Fig. 6a. Once significant transient IGW activity has left the vicinity of the forcing region, a partitioning of the total perturbation flow into geostrophic and ageostrophic components will be done similar to the partitioning done in Section 3 in order to identify the geostrophic and ageostrophic circulations induced by the zonal momentum forcing of eq. (8).

At this time ($t = 4$ h), the free surface displacement in the vicinity of the forcing center is dominated by an elongated, southwest to northeast oriented, region of positive h' colocated with the forcing center (Fig. 6b). The center of this localized region of positive displacement is flanked to its immediate northwest and southeast by regions of negative displacement, approximately 1600 km in diameter, whose centers are located at $\boldsymbol{r} = (-640, 480)$ km and $(960, -320)$ km. For $|\boldsymbol{r}| = (x^2 + y^2)^{1/2} \geqslant 3200$ km, outwardly propagating IGWs are evident. Since the radially propagating IGWs travel a distance of 3200 km in a period of 4 h, their phase speed is estimated to be $c_p \sim 3200$ km/4 h $= 222.22$ ms^{-1}. The magnitude of the upstream propagating wave of negative elevation in the free surface displacement is 3.24 m, while that of the downstream propagating wave is 2.93 m. The magnitude of the region of positive free surface displacement located at $\boldsymbol{r} = (0, 0)$ is 15.3 m, while the magnitude of the negative h' centers flanking the high pressure region are 3.44 m and 4.21 m for the northwest and southeast cells, respectively. This response in the free surface displacement is due to the influence of the Coriolis force as the perturbation mass field adjusts to the perturbation wind field as described in Section 3.

Fig. 7a shows $\mathbf{V}'$ superimposed on w' at $t =$ 24 h. At this time, the maximum winds characterizing the forced response have increased to 7.57 ms^{-1}. The center of the westerly zonal jet is located 80 km west of the forcing center, while the center of the easterly jet is located 560 km east of the forcing center. The convergence line separating the easterly and westerly zonal jets is now positioned at $x = 240$ km instead of at $x = 40$ km as it was at $t = 4$ h (Fig. 6a). The magnitudes of the westerly ($u' > 0$) and easterly ($u' < 0$) zonal jets (not shown) are ~ 8.78 ms^{-1} and -7.95 ms^{-1} at this time. As at $t = 4$ h, the westerly jet is flanked by localized regions of easterly zonal perturbation flow and the easterly jet by westerly zonal perturbation flow, whose centers are located 640 km north and south of the localized jet cores located

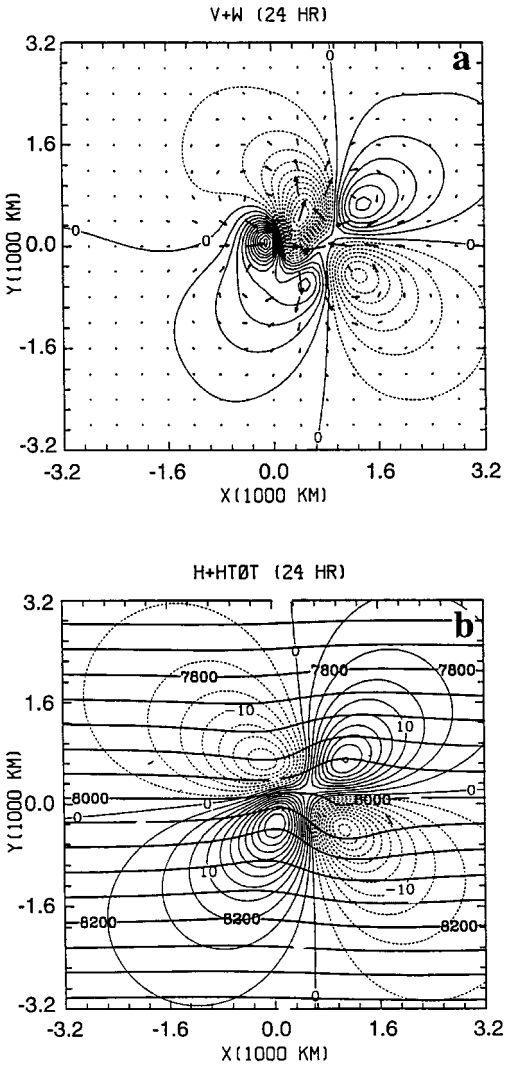

Fig. 7. Same as Fig. 6 except at $t = 24$ h. The maximum vector wind is 7.57 ms^{-1}. The contour interval for w' (h') is 7.0×10^{-5} ms^{-1} (3.0 m).

at $y = 0$. The magnitude of these compensating zonal counter currents are at this time approximately 2 ms^{-1} for both the easterly and westerly jets, and are part of the perturbation return flow around the dipoles in the free surface displacement field (Fig. 7b) which are becoming established to support the perturbation wind fields.

The w' field at $t = 24$ h (Fig. 7a) shows that a distinct four-cell pattern of vertical motion, roughly centered about $y = 0$, is forming approximately 1120 km east of the forcing center. The well-defined, localized regions of ascent and descent whose centers are located roughly 1600 km east and 640 km north and south of $y = 0$, have magnitudes of 2.8×10^{-4} ms^{-1}, and 3.5×10^{-4} ms^{-1}, respectively. The magnitude of the isolated cell of descent centered at $\boldsymbol{r} \sim (480$ km, 480 km) is approximately 5.93×10^{-4} ms^{-1}. In addition, at this time a well-defined localized cell of positive vertical motion is centered 160 km west of $\boldsymbol{r} = (0, 0)$, which has a magnitude of 6.24×10^{-4} ms^{-1}.

Isolated cells of positive h' exist to the southwest and northeast of the forcing center, while isolated cells of negative h' exist northwest and southeast of the forcing center, thereby forming a distinct four-cell pattern in the free surface displacement field at this time (Fig. 7b). The magnitude of the regions of negative h' in the northwest and southeast quadrants are 18 m and 27 m, respectively, while the magnitude of the regions of positive h' in the southwest and northeast quadrants are 30 m and 22 m, respectively. The isolated zonal jet west of the forcing center at $\boldsymbol{r} = (0, 0)$ shows evidence of the mass field adjusting to form a dipole of free surface displacement across the westerly zonal jet core. A similar adjustment process takes place as a dipole in the mass field forms to support the easterly zonal jet east of the forcing center, except that localized cells of positive and negative h' are reversed from those accompanying the westerly jet.

Fig. 8 shows $\mathbf{V}'_{ag}$ and $\delta' = (\partial u'/\partial x + \partial v')/\partial y)$ at $t = 24$ h. The ageostrophic component of the total perturbation flow shows that isolated cross-stream northerly meridional ageostrophic flow exists west of $\boldsymbol{r} = (0, 0)$, southerly meridional ageostrophic flow exists east of $\boldsymbol{r} = (0, 0)$ while isolated easterly and westerly zonal ageostrosphic flows exist north and south of $y = 0$ associated with a localized ageostrophic cyclonic circulation whose center is colocated with the forcing center. The maximum winds associated with this circulation are 2.79 ms^{-1} at this time. The magnitude of the geostrophic component of the perturbation flow is 7.9 ms^{-1} (not shown), and indicates that the dipole in h' which geostrophically balances the easterly zonal jet ($u' < 0$) east of the forcing center is more symmetric with respect to $y = 0$ than the mass dipole which balances the westerly zonal jet ($u' > 0$) west of the forcing center (Fig. 7b). The perturbation divergence field associated with the

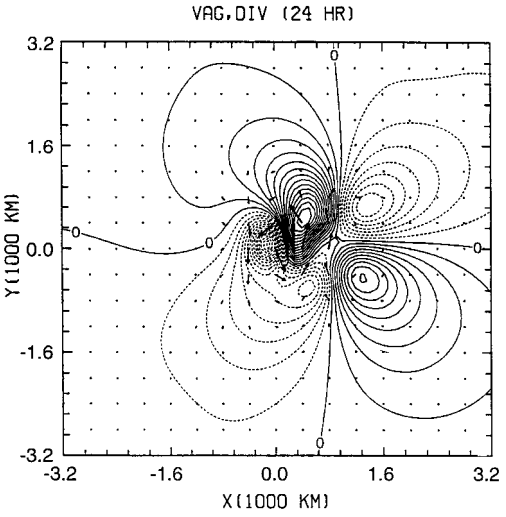

Fig. 8. Same as Fig. 3b except for the dipole forcing of eq. (8). The maximum ageostrophic vector wind is 2.79 ms^{-1}. The contour interval for δ' is 9×10^{-9} s^{-1}.

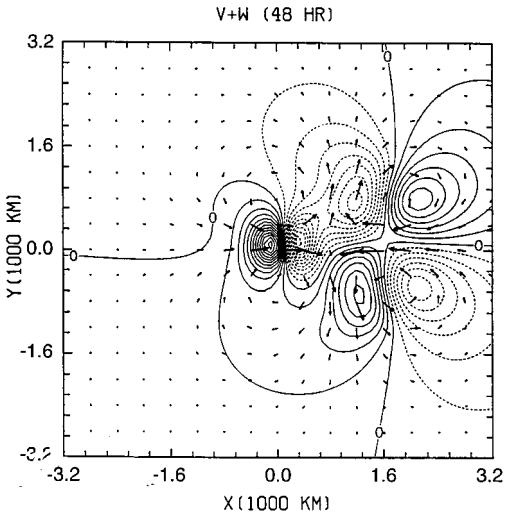

Fig. 9. Same as Fig. 4 except for the dipole forcing of eq. (8). The maximum total perturbation vector wind is 8.98 ms^{-1}. The contour interval for w' in panel is 7.0×10^{-5} ms^{-1}.

forced ageostrophic flow (Fig. 8) is the physical mechanism responsible for the developing field of vertical motion (Fig. 7a).

4.2. *Meso-α scale vertical motion associated with the easterly and westerly zonal winds*

By $t = 48$ h, the center of the easterly zonal wind perturbation is located at $x = 1600$ km in the forcing exit region, and is being advected downstream of the forcing center, leaving behind an isolated westerly zonal jet (Fig. 9). The core of this westerly jet is colocated with the center of zonal momentum forcing and is flanked by isolated regions of cyclonic and anticyclonic flow, respectively, north and south of the jet core. The magnitude of the maximum perturbation vector winds at this time is 8.98 ms^{-1}, while the magnitude of the westerly/easterly zonal jet is 9.64/8.92 ms^{-1}. The meridional wind perturbation at this time (not shown) shows evidence of well-defined confluence in the entrance region of the westerly jet streak as well as the exit region of the easterly jet, which can be inferred from $\mathbf{V}'$ (Fig. 9).

In the region between these two separating zonal wind anomalies, diffluence associated with the exit region of the westerly jet and entrance region of the easterly jet is becoming established. A dipole in free surface displacement with positive h' north of and negative h' south of $y = 0$ of magnitude 34.5 m and 42.5 m, respectively, is also being advected downstream and defines a portion of the total perturbation mass field which geostrophically balances the localized easterly zonal jet. The vertical motion associated with this downstream propagating perturbation defines a traditional four-cell pattern (in terms of conceptual jet streak models, e.g., Uccellini and Johnson, 1979) of ascent in the southwest and northeast and descent in the northwest and southeast quadrants flanking the core of the *easterly* zonal jet (Fig. 9). As the four-cell pattern of vertical motion is being carried downstream with this zonal flow anomaly, a new dipole of vertical motion is becoming established in the vicinity of the localized westerly zonal jet located at $\boldsymbol{r} = (0, 0)$. The magnitude of the isolated cell of rising motion is 6.3×10^{-4}, while that of the sinking cell is 4.9×10^{-4} ms^{-1}. At $t = 48$ h, w' shows evidence of both free (four-cell pattern traveling downstream) and forced (dipole colocated with forcing center) areostrophic circulations associated with the two separating zonal wind anomalies.

An analysis of $\mathbf{V}'_{ag}$ superimposed on the perturbation divergence field δ' (not shown) indicates that in addition to an asymmetric cyclonic circulation colocated with the forcing center, a weaker

ageostrophic perturbation exists downstream in the forcing exit region for 960 km $\leqslant x \leqslant$ 2400 km, roughly symmetric across $y = 0$. It is this weaker circulation in the forcing exit region which establishes the divergence responsible for the four-cell pattern of vertical motion associated with the isolated easterly zonal jet which is being advected downstream (Fig. 9). Furthermore, the divergence and convergence associated with the ageostrophic cyclonic circulation located at the origin is responsible for the dipole of vertical motion there.

4.3. *Meso-α scale flow response at day 4*

At $t = 96$ h, the center of the downstream advecting easterly zonal jet is located roughly 3200 km east of the forcing center (Fig. 10a), leaving behind a well-defined, isolated zonal jet whose perturbation vector winds are 9.42 ms^{-1}. The center of this isolated westerly zonal jet is colocated with the center of zonal momentum forcing, and has a core which is approximately 1280 km long and 640 km wide. The positive total zonal wind perturbation ($u' > 0$, not shown) has a magnitude of 10.2 ms^{-1}, and is flanked to the north and south by compensating easterly ($u' < 0$) zonal wind perturbations of 1.58 ms^{-1} associated with perturbation return flow about the dipole in free surface displacement (Fig. 10b) which geostrophically supports the localized zonal wind anomaly located at the forcing center. The region of negative free surface elevation north of and positive free surface displacement south of the zonal jet core have magnitudes of 29.6 and 39.0 m at this time (Fig. 10b). A similar mass dipole supports the downstream advecting easterly zonal jet, except that high surface elevation exists north of and low surface elevation exits south of $y = 0$. The meridional gradient $dH(y)/dy$ which supports the total zonal flow ($u = U + u'$) in the vicinity of the forcing center is approximately 13 m/100 km. The dipole of vertical motion w' (Fig. 10a), which indicates that ascent is occuring in the entrance region and descent in the exit region of the isolated zonal jet is better defined by this time than it was at $t = 48$ h (compare Figs. 9, 10a). Also evident at this time is a portion of the earlier four-cell pattern of vertical motion associated with the easterly zonal jet. The magnitude of the vertical motion dipole which is colocated with the forcing center is 5.6×10^{-4} ms^{-1}.

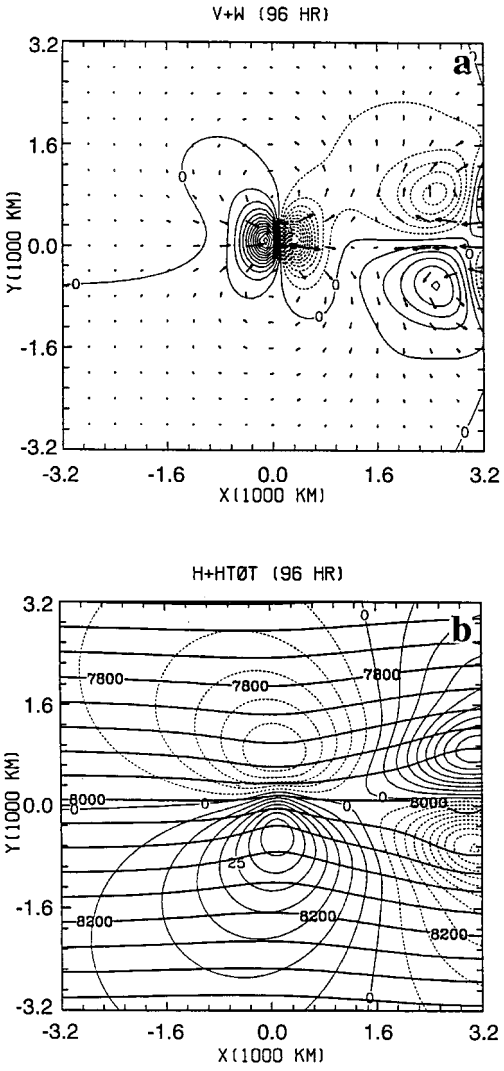

Fig. 10. Same as Fig. 2 except for the zonal momentum forcing of eq. (8) at $t = 96$ h. The maximum vector wind is 9.42 ms^{-1}. The contour interval for w' (h') is 7.0×10^{-5} ms^{-1} (5.0 m).

An analysis of the individual terms in eq. (3) (not shown) indicate which terms are dominant in producing w' at $t = 96$ h, although it should be remembered that the simulated vertical motion is simply a result of the convergence and divergence of the forced ageostrophic winds within the vicinity of the forcing region, compensated by ageostrophic flow which satisfies the continuity equation outside the forcing region. Similar to the results

produced by the isolated forcing of Section 3, advection of the free surface displacement by the relative basic state flow, $-(U-c)\,\partial h'/\partial x$, tends to partly cancel the contribution to the vertical velocity from the advection of the basic state height field by the meridional wind perturbation, $-v'\,\mathrm{d}H(y)/\mathrm{d}y$. A four-cell pattern in both of these physical terms becomes established in the vicinity of the forcing center located at $\boldsymbol{r}=(0,0)$ as well as 3200 km east of the forcing center. An easterly zonal jet is developing in the downstream region east of the forcing center due to the initial deceleration of the flow imposed by the prescribed momentum forcing.

Since high-low dipoles of free surface displacement form to support both the easterly and westerly zonal jets, the advection of the free surface displacement by the reduced basic state flow should develop this type of counterbalancing horizontal structure. Additionally, the four-cell pattern which develops downstream is almost a mirror image of the pattern which develops in the vicinity of the forcing center, since the mass dipole in h' downstream is reversed with respect to $y=0$ from the one at $\boldsymbol{r}=(0,0)$ (Fig. 10b). A four-cell pattern develops at the forcing center and further downstream in the $-v'\,\mathrm{d}H(y)/\mathrm{d}y$ field. This is a consequence of the entrance region confluence and exit region diffluence of the meridional wind perturbation accompanying the isolated westerly zonal jet, since in this particular study, the meridional gradient of the basic state height field, $\mathrm{d}H(y)/\mathrm{d}y$, is constant.

The contribution to w' from the nonlinear terms associated with the advection of the free surface displacement by the zonal and meridional wind perturbations show evidence of both free and forced responses. The free circulations are associated with the transient easterly zonal jet which is advecting downstream, while the forced circulation is colocated with the stationary zonal momentum forcing. Although the geometry of these terms are not identical, the zonal ($u'\,\partial h'/\partial x$) and meridional ($v'\,\partial h'/\partial y$) terms located at $\boldsymbol{r}=(0,0)$ as well as further downstream have a tendency to partially cancel each other's contribution to w'. The horizontal geometry which defines these nonlinear terms is a consequence of the structure of both the free surface displacement as well as the total zonal and meridional perturbation winds.

The linear divergence term, $-H(y)(\partial u'/\partial x+\partial v'/\partial y)$ (which has a dipole structure), dominates the nonlinear divergence term $-h'(\partial u'/\partial x+\partial v'/\partial y)$, (which exhibits a 4-cell pattern), particularly along the axis of maximum perturbation zonal wind, and is associated with the ageostrophic cyclonic circulation which is colocated with the forcing center (Fig. 8). Weglarz (1994) found that the vertical motion associated with the very weakly nonlinear (essentially linear) response for small perturbation Rossby number due to the impulsive introduction of a localized, unbalanced, zonal wind anomaly into a quiescent shallow water atmosphere was similar to the 4-cell nonlinear divergence mentioned above near $\boldsymbol{r}=(0,0)$ for $48\text{ h}\leqslant t\leqslant 96\text{ h}$, the period after which significant transient IGW activity had subsided.

Similar to isolated zonal momentum forcing, eq. (4), for the basic flow and forcing parameters adopted here, the vertical motion (Fig. 10a) is primarily the result of the linear divergence of the perturbation flow. The geostrophic and ageostrophic components of the total perturbation flow at this time, $t=96$ h (not shown), confirm that the isolated zonal jet at $\boldsymbol{r}=(0,)$ is an isolated geostrophic jet. The horizontal structure of the geostrophic wind vectors associated with the perturbation flow are similar to the total perturbation flow (Fig. 10a). The ageostrophic cyclonic circulation center is at this time still colocated with the center of zonal momentum forcing.

4.4. *Nonlinear response for meso-β scale dipole forcing*

The perturbation Rossby number defined by $R_{0,J}=u'_{\max}/fL_{\text{jet}}$ (Weglarz, 1994) associated with the meso-α scale jet of the previous section for $t\geqslant 96$ h is approximately 0.05. Since $R_{0,J}\ll[R_{0,U}=(U-c)/2af=0.1]$, nonlinear effects play no significant dynamical role in the adjustment dynamics for the problems addressed so far. We do not mean that nonlinearity is unimportant, rather that the nonlinear numerically simulated response is very similar to corresponding linear numerical simulations for the basic state flow and forcing parameters adopted in this study.

In order to investigate the role that stronger nonlinearity plays in adjustments driven by temporally continuous zonal momentum forcing in this simple model atmosphere, we perform an experiment with dipole forcing (eq. (8)), but where

the zonal and meridional half-widths, a and b, respectively, are both reduced to 100 km and the magnitude of the parameter u_{j0} is increased to 60 ms^{-1}. In this case the Rossby number as defined by the horizontal scale of the momentum forcing is $R_{0,U} = (U = c)/2af = 0.5$. The grid resolution in both spatial coordinates is taken to be 20 km, and the timestep is reduced to 10 s. The length scale of prescribed forcing ($\sim$200 km) will yield a response which should be more representative of forced meso-β scale adjustments in a rotating homogeneous atmosphere.

An analysis of the nonlinear response at $t = 4$ h (not shown) indicates that similar to meso-α scale forcing (Fig. 6a), isolated easterly and westerly zonal jets are produced east and west of the forcing center due to flow deceleration and acceleration produced in these regions by the prescribed momentum forcing. The magnitude of the perturbation flow at this time is approximately 8.5 times larger than that produced by meso-α scale forcing (Fig. 6a). Although the mass field still exhibits a SW-NE orientation similar to that produced by meso-α scale forcing (Fig. 6b), the response to meso-β scale forcing is dominated by a localized region of positive h' colocated with the forcing center, while a significant region of localized negative h' exists to its immediate southeast. These mass perturbations are responsible for producing a significant mesoscale ridge and trough in the basic height field. This mesoscale ridge is already present at $t = 1$ h, and is due to the strong flow convergence at the forcing center at that time (not shown) which is produced in the exit regions of the easterly and westerly zonal jets.

Since transient IGWs have propagated well beyond the forcing region by this time ($t = 4$ h), a partitioning of the total perturbation winds into geostrophic and ageostrophic components may be done. The analysis (not shown) indicates that the geostrophic winds essentially show the existence of two distinct mesoscale circulations. The first is a very asymmetric anticyclonic flow around the ridge colocated with the forcing center, while the second is a more symmetric cyclonic flow around the localized center of negative free surface elevation. A rather significant S-SW localized cross-stream geostrophic jet located 80 km south of $y = 0$ tends to separate the two circulations. Since the curvature associated with the mesoscale ridge and trough are quite significant, use of the geostrophic relationship tends to overestimate the circulation strength of the trough and underestimate the strength of the ridge, where a gradient wind analysis would yield better values. The forced ageostrophic winds show evidence of a divergent cyclonic flow which is approximately colocated with the forcing center at $\boldsymbol{r} = (0, 0)$. Localized convergence west and divergence east of the forcing center associated with the ageostrophic winds is responsible for producing localized regions of ascent and descent, respectively, which are developing.

At $t = 12$ h, better defined isolated easterly and westerly zonal jets exist, roughly symmetric about $y = 0$ whose cores are located at $\boldsymbol{r} \sim (420\text{ km}, 0)$ and $\boldsymbol{r} = (0, 0)$, respectively (Fig. 11a). The convergence line separating these two jets is located roughly 90 km downstream from the forcing center. The westerly jet is flanked by a cyclonic circulation whose center is located roughly 120 km north of the zonal jet core. Notice that a similar anticyclonic circulation exists south of the jet core. Similarly, the easterly jet is flanked by an anticyclonic circulation at approximately the same distance (120 km) north of $y = 0$, and a cyclonic circulation south of $y = 0$. The dipole in vertical velocity (Fig. 11a) with ascent in the jet entrance and descent in the jet exit region initially forms as early as $t \sim 4$ h.

The most dramatic difference between the response produced by meso-β scale forcing as compared to meso-α scale forcing used previously is evident in both the h' and $h = H(y) + h'$ fields (Fig. 11b). At $t = 12$ h, the perturbation mass field is dominated by two significant features. The first is a region of localized, positive free surface displacement centered at $\boldsymbol{r} \sim (15\text{ km}, -10\text{ km})$ which is skewed asymmetrically across the forcing center. The largest gradients associated with this disturbance occur north of $y = 0$, and therefore this feature may be defined as a mesoscale ridge in the basic height field, whose horizontal scale and amplitude are roughly 240 km and 8.032 km, respectively. The second feature is the localized region of negative surface elevation centered at $\boldsymbol{r} \sim (390\text{ km}, -125\text{ km})$. Since the center of the cyclonic circulation located south of $y = 0$ on the southern side of the easterly zonal jet (Fig. 11a) is colocated with this low pressure region, this feature may be defined as a *mesoscale cyclone*. The horizontal scale of this disturbance in the mass

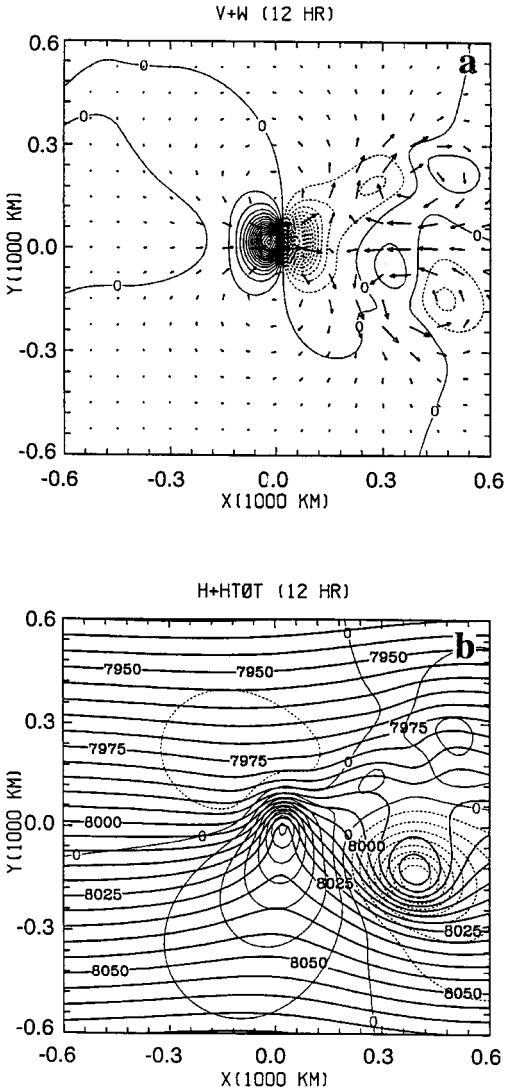

Fig. 11. Nonlinear response at $t = 12$ h to meso-β scale ($a = b = 100$ km, $u_{j0} = 60\ \mathrm{ms}^{-1}$) forcing whose geometry is given by Eq. (8). (a) $\mathbf{V}'$ superimposed on w', and (b) free surface displacement h' superimposed on total height field $h = H(y) + h'$. The maximum total perturbation wind is $15.7\ \mathrm{ms}^{-1}$. The contour interval for w' (h') *is* $9.0 \times 10^{-4}\ \mathrm{ms}^{-1}$ (4.0m).

field is approximately 300 km. The formation of this mesoscale cyclone can be explained as follows. Although the prescribed momentum forcing acts as a source/sink term for the perturbation potential vorticity, i.e.,

$$\frac{\mathrm{D}}{\mathrm{D}t}\left\{\frac{(\zeta' + f)}{[H(y) + h']}\right\} = \frac{F_\zeta}{[H(y) + h']}, \tag{9}$$

(where $F_\zeta = -\partial F_u/\partial y$ and $\mathrm{D}/\mathrm{D}t = \partial/\partial t + [(U - c) + u']\,\partial/\partial x + v'\,\partial/\partial y$), this mechanism will be dominant primarily over a circle of radius a, where a is the half-width of the forcing, centered at $\boldsymbol{r} = (0, 0)$. Outside of this region, the conservation relation, $\mathrm{D}/\mathrm{D}t\{(\zeta' + f)/[H(y) + h']\} \sim 0$, will be approximately valid. As fluid parcels are displaced northward, they end up in shallower fluid, while those that are displaced southward end up in deeper fluid, since $H(y) = H_0 - [f(U + c)/g]y$. As this happens, northward moving columns must shrink ($h < 0$), while southward moving columns must stretch ($h > 0$). In order for the potential vorticity to be conserved, columns displaced northward reduce their relative vorticity ($\zeta' < 0$), while those that move south increase their relative vorticity ($\zeta' > 0$). The combined NW-SE perturbation flow on the downstream side of the mesoridge combined with the NE-SW perturbation flow to the southwest of the easterly zonal jet is the physical mechanism responsible for displacing fluid parcels into deeper fluid, thereby increasing their relative vorticity which results in the formation of a mesocyclone in this region.

Figs. 12a and b show $\mathbf{V}'_{\mathrm{g}}$ and $\mathbf{V}'_{\mathrm{ag}}$ at $t = 12$ h, respectively. The perturbation divergence field δ' is also shown superimposed on $\mathbf{V}'_{\mathrm{ag}}$. A localized southwest to northeast oriented geostrophic flow (Fig. 12a) exists in the vicinity of the forcing center at $\boldsymbol{r} = (0, 0)$, and represents the induced flow around the mesoscale ridge in the height field which exists there (Fig. 11b). Since this perturbation flow is colocated with the localized region of positive h' displacement characterizing the mesoscale ridge in the height field, it can be defined as a *mesoscale anticyclone*. A well-defined cyclonic circulation exists further downstream to the southeast in the exit region of the prescribed zonal momentum forcing (Fig. 12a), and is associated with the developing mesoscale cyclone (Fig. 11b) on the southern side of the easterly zonal jet (Fig. 11a). The magnitude of the maximum geostrophic wind is $28.6\ \mathrm{ms}^{-1}$ at this time, and is associated with the wind vector whose head (tail) is located at $\boldsymbol{r} \sim (60, 90)$ km [$\boldsymbol{r} \sim (0, 60)$ km] which characterizes part of the perturbation flow around the mesoscale ridge in the free surface height field. The ageostrophic flow in the vicinity of the forcing

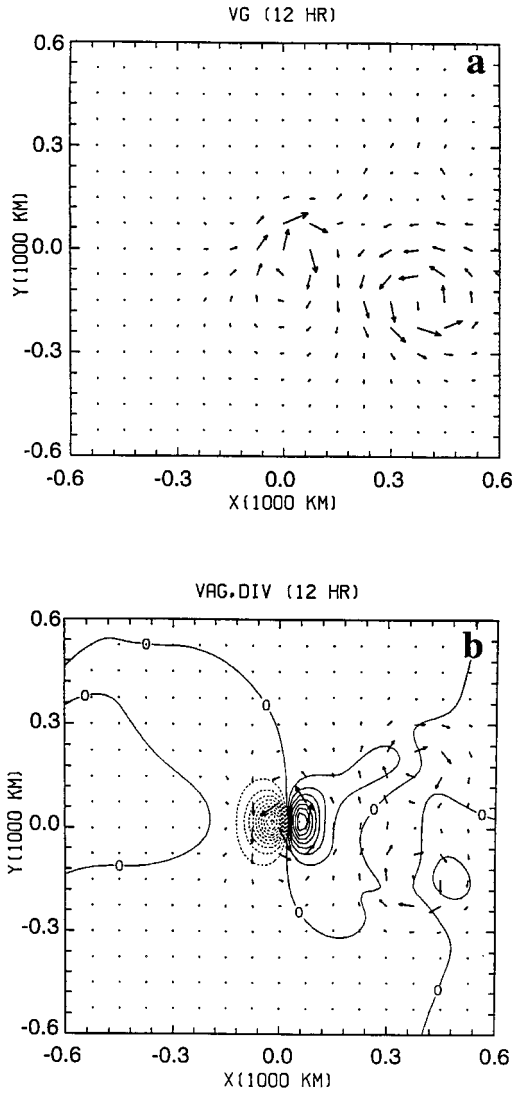

Fig. 12. Same as Fig. 11 except (a) $\mathbf{V}'_g$, and (b) $\mathbf{V}'_{ag}$ superimposed on perturbation divergence field δ'. The maximum geostrophic and ageostrophic perturbation winds are 28.6 and 24.0 ms^{-1}, respectively. The contour interval for δ' is 1.0×10^{-6} s^{-1}.

center exhibits an asymmetric, divergent cyclonic circulation (Fig. 12b), while further downstream a dipole pair of anticyclonic circulations exist north and south of $y = 0$. The divergent nature of the cyclonic circulation is responsible for the dipole of vertical motion which exhibits ascent in the entrance region and descent in the exit region of the isolated westerly jet at $\boldsymbol{r} = (0, 0)$ (Fig. 11a).

Analysis of the nonlinear response to meso-β scale dipole forcing at $t = 48$ h (not shown) indicates that the horizontal structure of $\mathbf{V}'$, as well as the dipole of vertical motion characterizing ascent in the jet entrance and descent in the jet exit region, once the easterly jet and its accompanying ageostrophic circulations have been advected downstream beyond the forcing exit region, is similar to that produced by meso-α scale dipole zonal momentum forcing (Figs. 9, 10a). The maximum vector winds at this time are approximately 1.8 times greater than those associated with the westerly zonal jet at $t = 48$ h produced by the forcing of eq. (8) when $u_{j0} = 30$ ms^{-1} and $a = b = 500$ km (Fig. 9). The magnitude of w' is ~ 13.6 times larger than that associated with the zonal jet of Fig. 9. The length and width of the westerly jet colocated with the forcing center are approximately 360 and 160 km, respectively. The perturbation Rossby number is $R_{0,J} = u'_{max}/fL_{jet} \sim 0.46$, which is 5.74 times larger than $R_{0,J}$ associated with the westerly jet at $t = 48$ h induced by the larger meso-α scale dipole forcing of the preceeding section.

At this time ($t = 48$ h) the transient easterly zonal jet induced by meso-β scale dipole forcing has been advected well downstream leaving behind an isolated westerly zonal jet colocated with the forcing center. For meso-α scale dipole forcing, the easterly jet is still a significant part of the total perturbation flow at $t = 48$ h (Fig. 9). By the time it is advected well downstream of the forcing center ($t > 96$ h) and the quasi-steady westerly jet becomes isolated, $R_{0,J}$ associated with the meso-β scale westerly jet is roughly 9.2 times greater than that associated with the meso-α scale jet. Additionally, it should be noted that due to stronger nonlinear accelerations, $-\mathbf{V}' \cdot \nabla \mathbf{V}'$, produced by meso-$\beta$ scale dipole forcing as compared to meso-α scale dipole forcing, the meso-β scale westerly jet colocated with the forcing center (Fig. 11a) forms roughly four times sooner than the meso-α scale westerly jet (Fig. 9).

Van Tuyl and Young (1982) demonstrated, using an idealized two-layer baroclinic channel model and an isolated jet streak of constant length, that the traditional four-cell pattern of vertical motions in jet streak entrance and exit regions are dramatically altered as the jet core strength

increases and the quasi-geostrophic jet streak flow approaches the IGW regime. Our numerical results showing *similar* vertical motions for perturbation Rossby numbers *which differ by almost an order of magnitude* is a specific signature of the continually forced problem that we are addressing here.

The evolution of jet streak ageostrophic winds and the corresponding vertical motions due to nonlinear advection in the absence of temporally continuous zonal momentum forcing for homogeneous and continuously stratified flows (Weglarz, 1994) more accurately reflects the true nature of midlatitude jet streak secondary circulations than those presented here. This should be kept in mind if these shallow water model results are applied to real atmospheric jet streak flows. $\mathbf{V}'_g$ and $\mathbf{V}'_{ag}$ at $t = 48$ h are similar to those shown in the vicinity of the forcing center at $t = 12$ h (Figs. 12a, b), except that the transient mesoscale cyclone in $\mathbf{V}'_g$ and dipole of anticyclonic flow in $\mathbf{V}'_{ag}$ have been advected downstream by the uniform basic state flow.

5. Summary

In this paper, we have investigated, using a simple shallow water model, the nonlinear hydrostatic response and subsequent adjustment of a uniform, geostrophically balanced, barotropic zonal flow in a homogeneous atmosphere of finite depth which is perturbed by two different types of downstream propagating meso-α/β scale momentum forcings. The prescribed isolated and dipole zonal momentum forcings represent, in a very simple and highly idealized manner, the effects of local momentum deposition or redistribution attributable to a variety of physical processes in the atmosphere.

For meso-α scale forcing, the early near-field response to either type of prescribed forcing (isolated or dipole) in the moving frame of reference for small Rossby number flow produces zonal wind perturbations whose geometries are similar to that of the imposed momentum forcing. Isolated forcing produces a localized meso-α scale westerly jet colocated with the forcing center, while dipole forcing produces localized meso-α scale westerly and easterly zonal jets west and east of the forcing center. The perturbation mass field adjusts to these disturbances in the wind field, since their horizontal scale is much less than the minimum Rossby radius of deformation. Although the vertical motion is dominated by transient inertia-gravity waves (IGWs) at early times, well-defined localized perturbations also begin to form in the vicinity of the forcing center. For isolated forcing, a dipole of vertical motion with ascent to the south and descent to the north of the forcing center forms. For dipole forcing, a four-cell pattern of vertical motion with ascent in the southwest and northeast and descent in the northwest and southeast quadrants adjacent to the forcing center forms.

At times greater than the advective time scale, $\tau = 2a/(U - c)$, the exit region of the zonal jet produced by isolated forcing is advected downstream at the relative speed $U - c$, carrying portions of the meridional perturbation winds and free surface displacement fields with it. A dipole of vertical motion with ascent to the south and descent to the north of $y = 0$ is associated with the ageostrophic circulation in the jet exit region. The long term asymptotic response is a downstream-extending zonal jet due to the advection by the uniform basic state flow of the temporally continuous relative vorticity deposited by the prescribed momentum forcing. The forced ageostrophic response consists of a cross-stream northerly flow in the jet entrance region. The divergence of this cross stream flow yields a region of upward motion colocated with the forcing center, compensated by weaker regions of subsidence to the east and west.

Also for $t > \tau$, the easterly jet produced by localized flow deceleration east of the forcing center associated with meso-α scale dipole forcing is advected downstream at the relative speed $U - c$, and is supported by a dipole of free surface displacement. A four-cell pattern of vertical motion accompanies this downstream advecting easterly jet. The quasi-steady equilibrium response in the vicinity of the forcing center is an isolated meso-α scale westerly jet, with meridionally confluent flow in its entrance region and diffluent flow in its exit region. A mass dipole supports this forced localized zonal flow perturbation. The ageostrophic flow accompanying this jet is a divergent cyclonic circulation, which produces rising motion in the jet entrance region, and sinking motion in the jet exit region.

For meso-β scale dipole forcing, a mesoscale

ridge forms in the vicinity of the forcing center while a mesoscale trough forms downstream to the southeast. The trough is a transient feature which intensifies with time, developing into a mesoscale cyclone which is advected downstream by the reduced basic state zonal flow. The quasi-steady equilibrium response within the vicinity of the forcing center is an isolated meso-β scale westerly jet, whose perturbation Rossby number $R_0 = u'_{\text{jet,max}}/fL_{\text{jet}}$ is larger than that associated with the westerly zonal jet induced by meso-α scale forcing. Stronger nonlinear advection allows the westerly jet to form four times sooner than the westerly jet produced by smaller Rossby number meso-α scale dipole forcing. The horizontal structure of the vertical motion associated with this isolated meso-β scale jet is identical to that produced by meso-α scale dipole forcing. This similarity in the vertical motion field for zonal jet perturbations whose Rossby numbers differ by almost an order of magnitude is a consequence of the temporally continuous zonal momentum forcing adopted in this study, rather than the development of nonlinear accelerations which evolve gradually in the absence of prescribed forcing.

In order to better understand the geostrophic adjustments associated with the fully nonlinear initial-value problem, the study presented here should be repeated in the absence of continuous prescribed forcing. Of particular importance will be the structure and evolution of the vertical motions and ageostrophic winds for localized zonal jets characterized by moderate (~ 0.5) to large (~ 1.0) perturbation Rossby numbers. These ageostrophic winds and vertical motions associated with nonlinear accelerations can be dramatically different from those produced by the temporally continuous forcing used in this study.

In addition, the geostrophically balanced zonal current should possess a lateral shear profile, $U = U(y)$, that is more representative of the true geometry of the polar and subtropical jet streams. For this type of basic state flow in a two-layer homogeneous atmosphere, the inertia-gravity waves (IGWs) generated can be influenced by critical latitudes (Geisler and Dickinson, 1972), and may be trapped in the vicinity of the jet core leading to a prolonged period of geostrophic adjustment. Wave trapping and the excitation of Rossby waves may also occur if the β effect is included. These mechanisms can significantly alter the nature of the final balanced equilibrium, and are physically more realistic processes for constraining transient IGWs to remain in the vicinity of their source region and interact with the mean flow rather than the adoption of artificial channel walls used in some studies.

6. Acknowledgments

The authors would like to sincerely thank Drs. Michael L. Kaplan and Gerald S. Janowitz at NC State Univerity, and Dr. Glen Shutts at the University of Reading, England for interesting discussions and for offering valuable comments on this work. We also would like to thank Dr. Hye-Yeong Chun at Yonsei University, Korea for her help with NCAR graphics software, and Tricia McKellar at NC State University for helping finalize the figures. Comments by several anonymous reviewers greatly improved the final draft of the manuscript. This work is funded under US Air Force grant F49620-95-1-0226, NASA research grant NAG5-1790-21, NSF grant ATM-9224595, and constitutes an extension of some of the work presented in the first author's PhD dissertation. The numerical simulations were performed on the North Carolina Supercomputing Center's Cray C90 and on the IBM-funded FOAM^{V} workstations at North Carolina State University.

REFERENCES

Andrews, D. G. and McIntyre, M. E. 1976. Planetary waves in horizontal and vertical shear. The generalized Eliassen-Palm relation and the mean zonal acceleration. *J. Atmos. Sci.* **33**, 2031–2048.

Asselin, R. A. 1972. Frequency filter for time integrations. *Mon. Wea. Rev.* **100**, 487–490.

Blumen, W. 1972. Geostrophic adjustment. *Rev. Geophys. Space Phys.* **10**, 485–528.

Cahn, A. 1945. An investigation of the free oscillations of a simple current system. *J. Meteor.* **2**, 113–119.

Challa, M. and Pfeffer, R. L. 1980. Effects of eddy fluxes of angular momentum on model hurricane development. *J. Atmos. Sci.* **37**, 2031–2048.

Geisler, J. E. and Dickinson, R. E. 1972. The role of variable Coriolis parameter in the propagation of iner-

tia-gravity waves during the process of geostrophic adjustment. *J. Phys. Ocean.* **2**, 263–272.

Gill, A. E. 1982. *Atmosphere-ocean dynamics*. Academic Press, 662 pp.

Montgomery, M. T. and Farrell, B. F. 1993. Tropical cyclone formation. *J. Atmos. Sci.* **50**, 285–310.

Pedlosky, J. 1987. *Geophysical fluid dynamics*. Springer-Verlag, New York, 710 pp.

Pielke, R. A. 1984. *Mesoscale meteorological modeling*. Academic Press, New York, 612 pp.

Rossby, C. G. 1938. On the mutual adjustment of pressure and velocity distributions in simple current systems (2). *J. Mar. Res.* **1**, 239–263.

Shapiro, R. 1970. Smoothing, filtering, and boundary effects. *Rev. Geophys. and Space Phys.* **8**, 359–387.

Shutts, G. J. 1994. The adjustment of a rotating, stratified fluid subject to localized sources of mass. *Quart. J. Roy. Meteor. Soc.* **120**, 361–386.

Shutts, G. J. and Gray, M. E. 1994. A numerical modeling study of the geostrophic adjustment process following deep convection. *Quart. J. Roy. Meteor. Soc.* **120**, 1145–1178.

Staniforth, A. N., Williams, R. T. and Neta, B. 1993. Influence of linear depth variation on Poincare, Kelvin, and Rossby waves. *J. Atmos. Sci.* **50**, 929–940.

Uccellini, L. W. and Johnson, D. R. 1979. The coupling of upper and lower tropospheric jet streaks and implications for the development of severe convective storms. *Mon. Wea. Rev.* **107**, 682–703.

Van Tuyl, A. H. and Young, J. A. 1982. Numerical simulation of nonlinear jet streak adjustment. *Mon. Wea. Rev.* **110**, 2038–2054.

Weglarz, R. P. 1994. *Three-dimensional geostrophic adjustment of homogeneous and continuously stratified atmospheres with application to the dynamics of midlatitude jet streaks*. PhD dissertation, North Carolina State University, 414 pp.

Weglarz, R. P. and Lin, Y.-L. 1997. A linear theory for jet streak formation due to zonal momentum forcing in a stably stratified atmosphere. *J. Atmos. Sci.* **54**, 908–932.

Zhang, C. 1993. Laterally forced equatorial perturbations in a linear model. Part II: Mobile forcing. *J. Atmos. Sci.* **50**, 807–821.

Zhang, C. and Webster, P. J. 1989. Effects of zonal flows on equatorially trapped waves. *J. Atmos. Sci.* **46**, 3632–3652.

Zhang, C. and Webster, P. J. 1992. Laterally forced equatorial perturbations in a linear model. Part I: Stationary transient forcing. *J. Atmos. Sci.* **49**, 585–607.

Zhu, X. and Holton, J. R. 1987. Mean fields induced by gravity-wave forcing in the middle atmosphere. *J. Atmos. Sci.* **44**, 620–630.